Advances in Nano Research, *Vol. 10, No. 6 (2021) 539-548*
DOI: https://doi.org/10.12989/anr.2021.10.6.539

Free vibration and buckling of functionally graded carbon nanotubes / graphene platelets Timoshenko sandwich beam resting on variable elastic foundation

Mohammad Mehdi Nejadi[1], Mehdi Mohammadimehr*[1] and Mojtaba Mehrabi[1,2]

[1]*Department of Solid Mechanics, Faculty of Mechanical Engineering, University of Kashan P.O. Box 87317-53153, Kashan, Iran*
[2]*Department of Solid Mechanics, Faculty of Mechanical Engineering, University of Isfahan, Isfahan, Iran*

(*Received November 5, 2020, Revised March 6, 2021, Accepted March 13, 2021*)

Abstract. Sandwich structures made of composites are widely applicable in different industries, including aerospace and power plants. The combination of a porous sandwich with functionally graded materials makes structures more resistant to analyze buckling and vibration behaviors. According to its high surface area and high strength, adding graphene platelets to the composite increases the final mechanical properties of composites. In the present paper, the effect of volume fraction distribution of fibers, numbers, and angles of layers in composites will be investigated. Additionally, the different porosity coefficients and distribution along the beam length will consider and the best porosity distributions will identify. Pasternak elastic foundation is considered during the beam length as linearly and parabolically. The equations of motion for the Timoshenko sandwich beam are solved by the differential quadrature method (DQM). The influences of adding graphene platelets with three various patterns on critical buckling load and natural frequency of composite beam will investigate. Also, the buckling and vibration behaviors of pure composites, perfect composite and FGM (Functionally Graded Material) composites will compare. Moreover, the critical buckling load will obtain by the Mori-Tanaka model.

Keywords: carbon nanotubes; graphene platelets; Timoshenko sandwich beam; porous core; DQM

1. Introduction

Porous materials are widely used in the structural design of vast number of fields and industries, including transportation, aerospace, energy, and construction, according to their low specific weight, and increasing machinability.

Porous materials with functional properties have some similarities with functionally graded materials. The porosity can cause a smooth or rough change in mechanical properties depending on some parameters such as porosity distributions and volume fraction of composite.

During the last several years, the problem of buckling of porous materials with varying properties has been discussed by many authors.

The nonlocal transverse vibrations of monolayer graphene beams on elastic substrates under magnetic plate loading were investigated by Murmu *et al*. (2013). They showed that the natural frequency increases with increasing magnetic loading and decreasing of a nonlocal parameter. They concluded that the effect of magnetic loading was lower at higher modes frequencies. Analui *et al*. (2013) investigated the bi-axial buckling and vibration of nanobeams by finite element method (FEM) for different boundary conditions. Linear free vibrations dependent on the size of the functional gradient beams based on the first-order shear deformation theory (FSDT) were proposed by Natarjan *et al*. (2012). The functionally graded material of beam structure was a function of the thickness of the beam according to its power function. They demonstrated that increasing the nonlocal parameter and decreasing the index of material variability decreases the natural frequency of the beam. Hosseini Hashemi *et al*. (2013) developed an analytical solution for the free vibration of circular and hollow functional graduated nanowires using Eringen's theory and FSDT. The elastic properties of the materials are varied as a function of the strength of the volume percentage with the thickness, while the Poisson ratio's is assumed to be constant. All frequencies decreased with increasing of nonlocal parameters, especially with increasing boundary hardness, increasing nanobeam stiffness, increasing material strength parameter. Ansari and Sahani (2011) studied the vibrational behavior of nanobeam couplings, considering the effect of surface tension based on classical beam theories and FSDT. They examined that the effect of surface stress using the classical beam theory and FSDT on the natural frequency of the nanobeam cannot be neglected. The main frequency of nanobeam increases with increasing the positive value of surface coefficients and decreases with a negative value.

Also, many researches have been done on the buckling and deflection of orthotropic graphite beams. The effect of small scale on the thermal buckling behavior of quadrupole orthotropic nanobeams placed in an elastic environment was investigated by Malekzadeh *et al*. (2011). They concluded that the thermal critical buckling load enhances

*Corresponding author, Professor,
E-mail: mmohammadimehr@kashanu.ac.ir

ISSN: 2287-237X (Print), 2287-2388 (Online)

with increasing the elastic parameters. The effect of scale parameter on the critical buckling load decreases with increasing diagonal plate angle.

Nowadays, nanomaterials have many applications in different fields due to their unique properties. One of these applications is their use as a reinforcement in polymer composite materials, which improves the mechanical and other properties of these composites. One of these reinforcements is carbon nanotubes (CNTs), which has attracted many researcher attentions.

They used a modified mixing model to determine the mechanical properties of the composite beam.

Magnucki *et al*. (2006) presented a mathematical model of plates based on nonlinear displacement functions in shear deformation theories. The assumed displacements in linear physical and geometrical relationships allowed the model to describe well the potential energy of plate. They also solved the FE plate model in Ansys software for better comparison. In another study, Magnucka-Blandzi (2008) found a solution of symmetric curvature and buckling of thin-walled circular plates. Their structure was assumed under uniform pressure loads as well as concentrated forces. The mechanical properties of isotropic porous material were considered with the variable thickness and also compared with the homogeneous plates. Jabari *et al*. (2013, 2014) studied the thermal buckling of thin circular plates made of porous materials. The effect of shear modulus is visible in different form of asymmetric porosity coefficients, nonlinear, and linear distributions. They concluded that the critical buckling temperature decreases with increasing porosity and instability of plate. Also, it was shown that the stiffness of plate is more symmetric in comparison of nonlinear symmetric distribution around the holes. Moreover, the position of the cavities in the porous materials is highly influenced by the shear strength and the buckling temperature. The buckling analysis of a solid rectangular plate made of porous materials with piezoelectric layers is investigated by Jabari and Rezaei (2016). Chen *et al*. (2015) hypothesized that in studying the elastic buckling and static bending of a beam, Young's modulus and density of porous composite would vary in thickness with two different patterns. Tang *et al*. (2018) studied the beam buckling analysis with a porosity in two perpendicular directions. The proposed beam model removes the defect of the porous beam model in one direction, which cannot show changes in mechanical properties in the axial direction. Moreover, they depicted that X-shaped porosity distribution is more sensitive in comparison of porosity volume percentage. Also, it was found that the critical buckling load sensitivity to the slip coefficient increases with increasing nodes number. Taborda *et al*. (2018) considered effective torsional strength of axially restricted RC beams. Radik (2018) studied the buckling of two-sided porous nanorods using nonlocal strain gradient elasticity (SGT) on Pasternak elastic foundation. Bilateral established behaviors of thin-layer nanostructured for the first time in the thermal medium. The nonlinear gradient theory with two material scale parameters are designed to investigate the bending behavior of nanostructure. He derived the equilibrium of equations based on shear deformation theory using the principle of minimum potential energy, and solved them using Galerkin method for various boundary conditions. Chikr *et al*. (2019) considered a new higher-order shear and normal deformation theory for the buckling analysis of new type of functionally graded material (FGM) sandwich plates. Anirood *et al*. (2019) performed a FEM bending, buckling and vibration analysis of porous graphene reinforced with curved beams. In their paper, the effects of various parameters such as porosity correlation, type of porosity pattern distribution on graphene plates (GPLs), the curvature radius of beam curve, the length-to-thickness ratio, GPLs geometry, and boundary conditions are investigated on the static bending and free vibration behavior of composite beam and presented their results for certain boundary conditions of GPLs-reinforced curved beams. Ebrahimi *et al*. (2019) illustrated buckling analysis of GPL oxide powder-reinforced nanocomposite beams subjected to non-uniform magnetic field. Using higher-order models, Polit *et al*. (2019) studied the bending and elastic stability of FG-GPLs reinforced porous nano-composite curved beams and investigated the effect of thick elongation. The structural properties of the curved beam, including porous metal foam and GPLs, evaluated as nano-fillers for reinforcement. Also, the curvature and stress distribution tested for thickness of beam. Gao *et al*. (2019) predicted nonlinear vibration of FG nanotubes using nonlocal SGT and a two-steps perturbation method. Arefi *et al*. (2019) studied the applications of nonlocal SGT in the flexural analysis of a sandwich porous nanoparticle with piezoelectric plates layers. Equations with different values used to change the porosity in direction of thickness. Nonlocal parameters related to the SGT used to describe the decrease and increase structure stiffness. Mohamed *et al*. (2019) depicted energy equivalent model in analysis of post-buckling of imperfect CNTs resting on nonlinear elastic foundation. Sobhy and Zenkour (2019) investigated the effects of porosity and heterogeneity on a two-dimensional nanostructure made of functionally graded materials using SGT. A new quasi-3D vector theory presented to model distances. This theory contained only five unknown functions and assumed that the shear strain increased with increasing thickness. Also, the numerical calculations performed to show the effects of the material size parameters. Mohammadimehr *et al*. (2020) and Mehrabi *et al*. (2021) investigated the vibration analysis of a sandwich composite micro porous Timoshenko beam model reinforced by CNTs and GPLs based on SGT using differential quadrature method (DQM). The effect of thickness on the mechanics of nanobeams is presented by Li *et al* (2018) using nonlocal SGT. Wave propagation, vibration, and bending behaviors of porous nanotubes are investigated by She *et al*. (2018, 2019) via nonlocal SGT. Buckling and free vibration analyses of annular thin sector plate made of FGMs resting on visco-elastic Pasternak foundation, subjected to the external radial, circumferential and shear in-plane loads are studied by Mohammadimehr *et al*. (2019). A four-unknown refined plate theory developed by Karimi and Karimi (2019) using Galerkin method to analyze the size-dependent stability behavior of FGM under

the thermal environment. Shahsavari *et al.* (2018) demonstrated shear buckling analysis of single layer GPLs based on the different nonlocal SGT. Bessaim *et al.* (2018) studied the mechanical buckling response of refined hyperbolic shear deformable FG nanobeams embedded in an elastic foundation based on the refined hyperbolic shear deformation theory. Akbas (2018) investigated the forced vibration analysis of FG porous deep beams under the dynamic load. It is found that changing the FG material in the thickness of sandwich beam has a great effect on the natural frequencies and therefore, can be used to control the natural frequencies by Li *et al.* (2016). Virtual strain energy function of shear beams contained additional nonlocal shear stress and high-order nonlocal shear stress related to the thickness direction in comparison with Euler–Bernoulli beam by Tang *et al.* (2019). Shariati *et al.* (2020) investigated vibrational behavior of GPLs under linearly varying in-plane bending load based on the nonlocal SGT. Akbaş (2020) studied modal analysis of viscoelastic nanorods under an axially harmonic load. Noroozi *et al.* (2020) considered torsional vibration analysis of bi-directional FG nano-cone with arbitrary cross-section based on nonlocal SGT elasticity. Nejadi *et al.* (2020, 2021) presented buckling analysis of nano composite sandwich Euler-Bernoulli beam considering porosity distribution on elastic foundation using DQM. In-plane bi-directional FG materials and geometrical imperfections is considered by Chen *et al.* (2021). The nonlinear parametric resonance behaviors of rotating composite laminated shells are investigated by Li (2021).

In the present study, the buckling and free vibration analyses of sandwich composite beam consist of Fiber Reinforced Composite (FRC) beam made of FGM, for various laminates with different angles and three models using DQM will be analyzed. Moreover, the influences of porosity coefficients, and porosity distribution types on critical buckling load and natural frequency, elastic foundation, volume fraction of GPLs, and their dispersion patterns will discuss.

2. Governing equations of motion for sandwich beam

The sandwich composite beam composed of a core and two layers in the top and bottom is resting on Pasternak foundation. The top and bottom layers are made of Carbon Fiber, and the core is made of glass fiber. Fig. 1 describes the present problem schematically with one layer for each part. Fig. 2 shows the chosen number of composite layers to analyze.

Also, three models are considered, which their fraction of core height to peripheral layer height is different as follows

Model 1: $\frac{H_c}{H_t} = 4/3$

Model 2: $\frac{H_c}{H_t} = 3$

Model 3: $\frac{H_c}{H_t} = 8$

While the total height of composite, and the numbers of layers are the same. In this paper, Model 3 is considered as the main model; otherwise it will be mentioned. To discuss the influence of angles on the buckling load and natural frequency, four laminates are defined in Table 1.

Functionally graded carbon nano tubes, and layers of beam are assumed as a continuous body. It is also assumed that no separation occurs between the carbon nanotubes, the matrix, and the layers during motion.

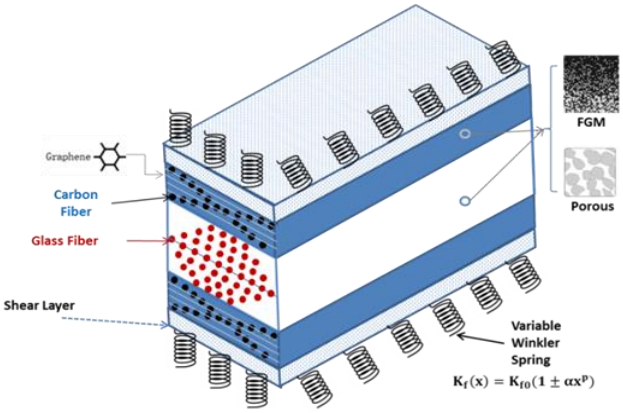

Fig. 1 Sandwich composite beam resting on elastic foundations with one schematic layer

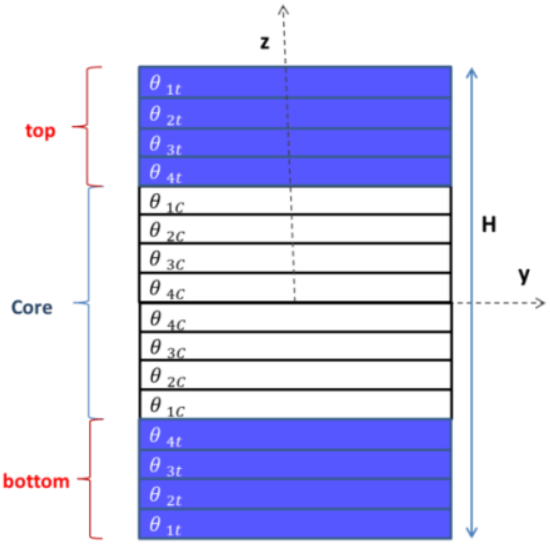

Fig. 2 Number of layers for core and top and bottom facesheets

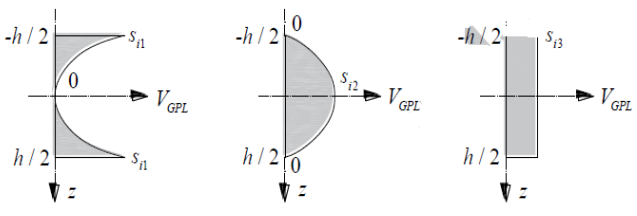

Fig. 3 Pattern distributions of graphene platelets (GPLs)

Table 1 The angles of sandwich Nano composite beam for Laminate 1, 2 and 3

Laminate	θ_{1t}	θ_{2t}	θ_{3t}	θ_{4t}	θ_{1c}	θ_{2c}	θ_{3c}	θ_{4c}
1	0	30	60	90	0	30	60	90
2	45	-45	45	-45	45	-45	45	-45
3	0	90	0	90	0	90	0	90

Based on free body diagram of a beam element presented by Timoshenko (1995), we have

$$\frac{dV}{dx} = -\rho A\ddot{w} + q(x,t) \tag{1}$$

$$V = \frac{dM}{dx} - P\frac{dw}{dx} - \rho I\frac{\partial^2\varphi}{\partial t^2} \tag{2}$$

where V is shear force, w is beam deflection, M is bending Moment, φ is rotation and

$$M = EI\ \partial\varphi/\partial x \tag{3}$$

$$V = KAG(\varphi - \partial w/\partial x) \tag{4}$$

Governing equation for Timoshenko composite beam are obtained as follows

$$KAG\left(\varphi - \frac{\partial w}{\partial x}\right) + P\frac{\partial w}{\partial x} + \rho I\frac{\partial^2\varphi}{\partial t^2} - \frac{\partial\left(EI\frac{\partial\varphi}{\partial x}\right)}{\partial x} = 0 \tag{5}$$

$$\frac{\partial[KAG\left(\varphi - \frac{\partial w}{\partial x}\right)]}{\partial x} + \rho I\frac{\partial^2 w}{\partial t^2} = q(x,t) \tag{6}$$

where K as shear correction factor is considered to be 5/6, according to the rectangular cross-section, P_{cr} is the critical buckling load, $q(x,t)$ is an external force, I is moment of inertia for the cross-section, A is cross-section area, ρ is density, ω is circular natural frequency, K_f (x) is spring constant, which could be constant or vary linearly or parabolically through the length of the beam as follows

$$K_f(x) = K_{f0} \qquad Constan \tag{7}$$

$$K_f(x) = K_{f0}(1 - \alpha x) \qquad Linear \tag{8}$$

$$K_f(x) = K_{f0}(1 - \alpha x^2) \qquad Parabolic \tag{9}$$

E_{ef} is the effective modulus of elasticity, which can be presented as follows

$$E_{ef} = \frac{8}{h^3}\sum_{j=1}^{\frac{m}{2}}(E_x)_j\,(z_j^3 - z_{j-1}^3) \tag{10}$$

where m is the number of layers, h is the height of the beam, z is the distance between the outer plane of the jth layer and the neutral axis. According to the importance of shear in Timoshenko theory, G_{ef} has the similar equation.

Dimensionless critical buckling load can be obtained as

$$N_{cr} = \frac{P_{cr}}{A_{110}} \tag{11}$$

where A_{11} expressed by Eq. (11) is extensional stiffness of beam, and A_{110} represents A_{11} for the beam made of the pure matrix.

$$A_{11} = \sum_{k=1}^{n}\int_{h_{k-1}}^{h_k}(Q_{11}cos^4\theta + Q_{22}sin^4\theta + (2Q_{12} + 4G_{12})sin^2\theta cos^2\theta)_k\,dz \tag{12}$$

In the mentioned equation, h_k and h_{k-1} are the z values for the top, and bottom, respectively. Also, the stiffness elements are considered as follows

$$Q_{11} = \frac{E_1}{1 - v_{12}v_{21}} \tag{13}$$

$$Q_{22} = \frac{E_2}{1 - v_{12}v_{21}} \tag{14}$$

$$Q_{12} = \frac{v_{12}E_2}{1 - v_{12}v_{21}} \tag{15}$$

3. Solving method

To solve the equations by DQM, the first–order, the second–order, the third-order and the fourth derivatives of an arbitrary function in arbitrary point can be approximated in all intervals as follows

$$\frac{d^r f}{dx^r}(x = x_i) = \sum_{k=1}^{n} A_{ik}^r f(x_k) \tag{16}$$

where A^r is weighted coefficient matrices which are defined by Eqs. (17), (18) and (19).

$$A_{ij}^{(1)} = \frac{\prod_{m=1}^{m\neq i,j}^{N}(x_i - x_m)}{\prod_{m=1}^{m\neq j}^{N}(x_i - x_m)} \qquad (i,j = 1,2,3,\dots,N; i \neq j) \tag{17}$$

$$A_{ij}^{(1)} = \sum_{\substack{m=1\\ m\neq j}}^{N}\frac{1}{(x_i - x_m)} \qquad (i,j = 1,2,3,\dots,N) \tag{18}$$

$$A^r = A^{(r-1)}A^r \qquad 2 \le r \le N-1 \tag{19}$$

Chebyshev points which are a well-recognized set of the grid points for the interval [0, L] are presented as follows

$$x_i = \frac{1}{2}\left\{1 - cos\left[\frac{(i-1)\pi}{(N-1)}\right]\right\} \tag{20}$$

4. Material properties

The mechanical properties of nanocomposite beam made of fiber reinforced polymer can be estimated using the

extended rule of mixture in Eqs. (21) to (24) (Gui *et al*. 2011). The elastic properties of PMMA matrix, carbon fiber, and glass fiber are listed in Table 2. Young's Modulus of three-phase composite (Graphene Platelet added to composite) could be obtained from Eq. (25). Other mechanical properties such as shear modulus and Poison's ratio are similar. The PMMA, supplied as beads, is dissolved in chloroform at different concentrations to make porous matrix in different porosity types.

As presented in Fig. 1, fibers are distributed along the matrix in four conditions (Eq. (26)) to explore the best combination. It should be mentioned that volume fractions of fibers are considered to be 0.4.

$$E_{11} = V_f E_{11}^f + (1 - V_f) E^m \tag{21}$$

$$\frac{\eta_2}{E_{22}} = \frac{V_f}{E_{22}^f} + \frac{V_m}{E^m} \tag{22}$$

$$\frac{\eta_3}{G_{12}} = \frac{V_f}{G_{12}^f} + \frac{V_m}{G^m} \tag{23}$$

$$v_{12} = V_{CNT} v_{12}^{CNT} + V_m v^m \tag{24}$$

Moreover, Graphene platelets can be used to construct a variety of carbon-based nanostructures (Rafiee *et al*. 2009). To model the elastic modulus of the graphene platelets nanocomposites, it is assumed that GPLs act as an effective rectangular solid fiber with width (b_{GPL}), length (a_{GPL}), and thickness (t_{GPL}) (Halpin and Tsai 1967). To predict elastic properties, the Halpin-Tsai equations were modified for the GPL nanocomposite as follows

$$E_{GPLC} = \frac{3}{8}\frac{1 + \varepsilon_L \eta_L V_{GPL}}{1 - \eta_L V_{GPL}} E_m + \frac{5}{8}\frac{1 + \varepsilon_T \eta_T V_{GPL}}{1 - \eta_T V_{GPL}} E_m \tag{25}$$

where

$$\eta_L = \frac{(E_{GPL}/E_m) - 1}{(E_{GPL}/E_m) + \varepsilon_L}, \qquad \eta_T = \frac{(E_{GPL}/E_m) - 1}{(E_{GPL}/E_m) + \varepsilon_T} \tag{26}$$

The parameter ε depends on the geometry and boundary conditions of the effective fiber. According to Halpin and Tsai (1967) for rectangular filaments, the parameter ε can be expressed as follows (Rafiee *et al*. 2009)

$$\varepsilon_L = 2\frac{a_{GPL}}{t_{GPL}} \tag{27}$$

$$\varepsilon_T = 2\frac{b_{GPL}}{t_{GPL}} \tag{28}$$

where a_{GPL}, b_{GPL}, and t_{GPL} are length, width, and thickness of GPLs, respectively. It is seen that with an increase of length and width of GPLs, the stiffness of sandwich structures increases; while this results for thickness of GPLs is vice versa.

The geometrical sizes of the GPL are considered to be: t_{GPL} = 1.5 nm, b_{GPL} = 1.5 μm, a_{GPL} = 2.5 μm.

Since in the present paper, glass fibers plus graphene platelet are used in the matrix, Young's modulus of the three-phase composite can be calculated by Eq. (25).

Table 2 The angles of sandwich nano composite beam for Laminate 1, 2 and 3

Material	E_{11} (*GPa*)	E_{12} (*GPa*)	G_{12} (*GPa*)	V_{12}
PMMA	2.5	2.5	0.933	0.34
Carbon Fiber	600	14	9	0.2
Glass Fiber	73.1	5	30	0.22

$$E_{11}^{Three-Phase} = V_f E_{11}^f + (1 - V_f) E_{GPLC} \tag{29}$$

Dispersion Patterns of Graphene Platelets (Fig. 3) are defined as follows

$$V_{GPL} = \begin{cases} V_f^* \left(1 - \cos\left(\frac{\pi z}{h}\right)\right) & \text{(Pattern A)} \\ V_f^* \left(1 - \cos\frac{\pi}{2}\left(\frac{z}{h} + \frac{1}{2}\right)\right) & \text{(Pattern B)} \\ V_f^* & \text{(Pattern C)} \end{cases} \tag{30}$$

Pattern C corresponds to an isotropic homogenous plate in which GPLs are uniformly distributed at the same volume fraction across all layers, while in other patterns, GPL weight fraction changes. In Pattern B, GPL volume fraction decreases from the highest in the mid-plane to the lowest on both top and bottom surfaces of the plate, but it is precisely reversed with the maximum volume fraction on both top and bottom surfaces and the lowest in the mid-plane of the plate in pattern A.

Distribution of fibers during the matrix is considered to be in four conditions presented in Eqs. (31)-(34). The composite material is considered a mixture of uniaxially aligned single-walled fibers and isotropic matrix in which material properties are continuously varied along the thickness direction. Besides the uniform distribution of fibers through the thickness direction of composite material, the other three types of functionally graded distributions of fibers are taken into consideration, which is denoted by FGA, FGO, and FGX, in which the inner surface, the mid-plane and both inner, and outer surfaces of the shell are fiber-rich, respectively.

$$V_f = \begin{cases} V_f^* & \text{(U. D.)} \quad (31) \\ V_f^* \left(1 + 2\frac{z}{h}\right) & \text{(F. G} - \text{A)} \quad (32) \\ V_f^* \left(4\frac{|z|}{h}\right) & \text{(F. G} - \text{X)} \quad (33) \\ V_f^* \left(2 - 4\frac{|z|}{h}\right) & \text{(F. G.} - \text{O)} \quad (34) \end{cases}$$

For adding porosity consideration, the elastic properties of a matrix of the composite are assumed to vary by two types of porosity distribution across the height. Porosity distribution types are presented by the left side of Eqs. (21) to (23) as described earlier. The right side of mentioned equations shows the effect of FGM with a different distribution.

$$Efgm = (-E1)\left(\frac{z}{h} + \frac{1}{2}\right)^q + E1 \tag{35}$$

$$1:\ E(z) = E_0\left[1 - e_1\left(cos\left(\frac{\pi}{h}\right)z\right)\right] + Efgm \quad (36)$$

$$2:\ E(z) = E_0\left[1 - e_1\left(1 - cos\left(\frac{\pi}{h}\right)z\right)\right] + Efgm \quad (37)$$

$$3:\ E(z) = E_0\left[e_1\left(\frac{z}{h} + \frac{1}{2}\right)\right] + Efgm \quad (38)$$

where E_1 and E_0 are Young's modulus of elasticity, e_1 is the coefficient of beam porosity, q is the gradient index of FG material. It should be mentioned that the same pattern is considered for shear modulus, Poisson's ratio, and density.

In the case of zero porosity coefficient, there is no porosity, and all points of matrix have the same Young's modulus; while when the porosity coefficient is equal to 1, the maximum porosity occurs between two layers. In case of gradient index equals zero, the material will be pure. All conditions are briefed in Table 3.

5. Result and discussion

5.1 Results and discussion of buckling

Dimensionless critical buckling load of CNTRC (Carbon Nano Tube Reinforced Composite) with and without elastic foundations is presented in Table 4. The buckling loads are compared with the results of Yas and Samadi (2012) for three volume fractions of carbon nanotube. As can be seen, the resulted data are consistent. The comparisons between the present work and Chen *et al*. (2017) for homogeneous core and nanocomposite facesheets are shown in Table 5. To validate the obtained results from this research for first and second natural frequencies with Chen *et al*. (2017), it is shown that there is a good agreement between them.

To investigate the effect of porosity distribution on critical buckling load, three general types of distribution are considered. Critical buckling loads among slender ratio of the beam for three laminates described in Table 1 and three models mentioned earlier in the problem statement can be seen in Table 6. Model 3 has the most critical buckling load. Among the three laminates, laminate 1 is incredibly more resistant against buckling.

It is evident from Fig. 4, although the beginning point of the three curves is the same because of no porosity, the differences rise by increasing the porosity coefficient. It also can be seen that by considering distribution Type 2, the beam gives the most resistance against buckling due to increasing the stiffness of the Timoshenko beam. When the middle of the beam has the minimum stiffness and outer layers have more Young's Modulus, the structure is stronger against buckling, which occurs at the farthest distance from the neutral axis because of bending moments. In contrast, the beam with the distribution of porosity Type 1 is the least resistant one.

As can be seen in Fig. 4, porous composite has the least critical buckling load comparing to the others mentioned in Table 3. Considering porosity leads to a decrease in the stiffness of structure. The second place belongs to Perfect Composite, which is only stronger than porous composite.

Table 3 FGM and Porous parameters

Material	Parameters
Porous Composite	q = 0, 0 < e1 < 1
Perfect Composite	q = 0, e1 = 0
Porous FGM	$q \neq 0$, 0 < e1 < 1
Perfect FGM	$q \neq 0$, e1 = 0

Table 4 The comparison between the present work and the obtained results by Yas and Samadi (2012) for critical buckling load in aspect ratio 15

V^*_{cnt}	CNT Distribution	$\bar{N}_{cr} \times 10$ Present Work	$\bar{N}_{cr} \times 10$ Yas and Samadi (2012)	Difference (%)
0.12		1.65	1.82	9.14
0.17	FGA	2.60	2.88	9.71
0.28		3.68	3.99	7.87
0.12		2.26	2.46	8.21
0.17	FGX	3.83	4.04	5.15
0.28		4.89	5.33	8.16
0.12		1.52	1.57	3.34
0.17	FGO	2.58	2.45	5.38
0.28		3.66	3.58	2.40

Table 5 The comparisons between the present work and Chen *et al*. (2017) for homogeneous core and nano-composite facesheets

Axial number of frequency(n)	1	2
Present work	0.1378	0.5442
Chen *et al*. (2017)	0.1432	0.5650

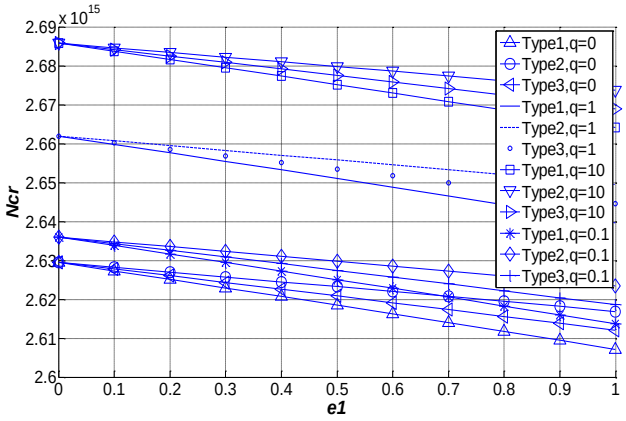

Fig. 4 Comparison of FGM composite with pure composite in different porosities

By increasing the gradient index of FG material in Perfect FGM leading to more stiffness, the critical buckling load will rise substantially. It is concluded that the functionally graded material increases the stiffness of the structure, it is

more effective than reducing weight by porosity. As was expected, Porous FGM has less buckling load than the perfect one because of less stiffness.

The curve of critical buckling load versus volume fraction of graphene platelet in three various patterns is presented in Fig. 5. It is shown because of the more strength, the beam by increasing the volume percentage of graphene porosity, the critical buckling load increases. On the other hand, with an increase in the volume fraction of graphene platelet, the critical buckling load because increasing the stiffness of sandwich structures enhances. Pattern A (symmetric with the minimum graphene in the middle of the beam) has the least resistant against buckling. In contrast, Pattern B (which is symmetric but has the maximum graphene in the middle) has the most resistance. By increasing the porosity coefficient, the critical buckling decreases slightly.

As can be seen in Fig. 6, by increasing the thickness of GPLs, critical buckling load reduce slightly. It is also seen the width and length of GPLs have the reverse effect on the critical buckling load. In all three subfigures, while volume fraction of GPLs rises, the differences between the curves become more noticeable.

Table 6 Critical buckling load for different laminates and models

Composite Specification		L/H	Ncr
Model 1	Laminate 1	10	2.02E+18
		20	5.05E+17
		30	2.24E+17
	Laminate 2	10	2.84E+16
		20	7.10E+15
		30	3.16E+15
	Laminate 3	10	2.70E+00
		20	6.74E+00
		30	3.00E+00
Model 2	Laminate 1	10	6.85E+18
		20	1.71E+18
		30	7.61E+17
	Laminate 2	10	1.41E+17
		20	3.53E+16
		30	1.57E+16
	Laminate 3	10	9.11E+00
		20	2.28E+00
		30	1.01E+00
Model 3	Laminate 1	10	1.63E+19
		20	8.24E+16
		30	8.14E+17
	Laminate 2	10	3.81E+16
		20	9.51E+15
		30	8.67E+15
	Laminate 3	10	2.16E+00
		20	5.41E+00
		30	2.40E+00

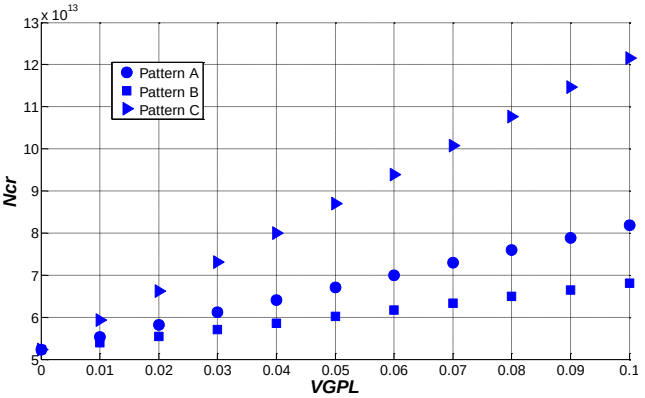

Fig. 5 Critical buckling load for different porosity types and graphene platelets patterns

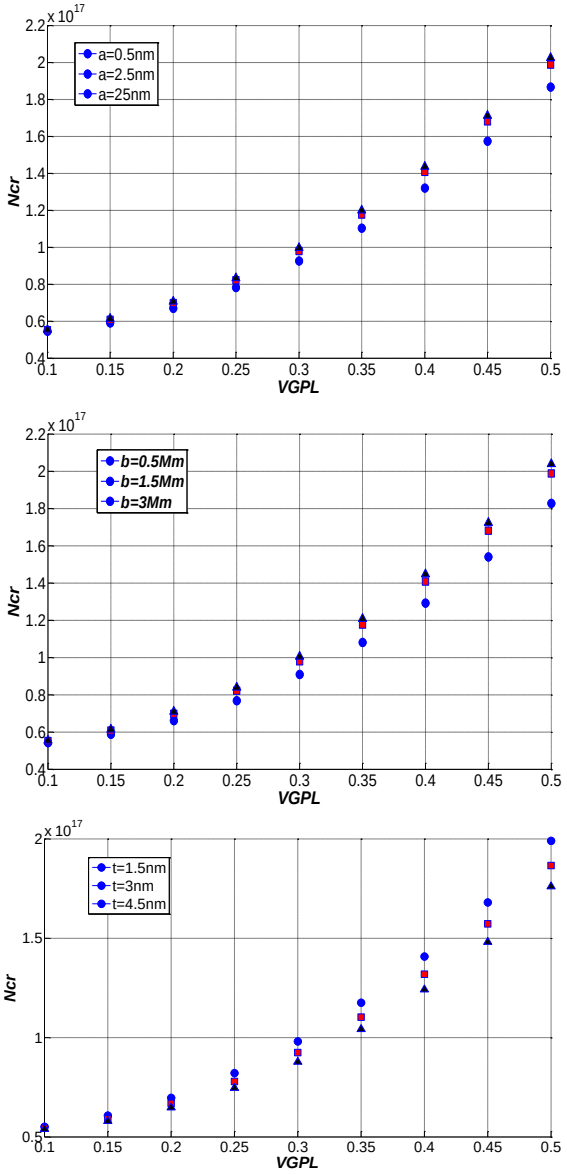

Fig. 6 The effects of geometrical sizes of the graphene platelet on the critical buckling load

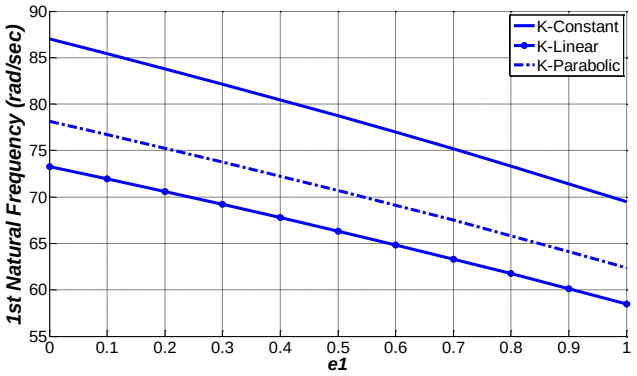

Fig. 7 First natural frequency against porosity coefficient for three kind of elastic foundations

Table 7 Natural frequency for different combination of core and top and bottom parts of composite

L/H	e_1	Order	ω(rad/sec) $\times 10^6$	Order	ω(rad/sec) $\times 10^6$
	0		10.34		11.70
10	0.5		9.91		11.27
	1		9.35		10.65
	0		7.31		8.28
20	0.5	FGO/FGX/FGO	7.01	FGA/FGX/FGA	7.97
	1		6.61		7.53
	0		5.97		6.76
30	0.5		5.72		6.51
	1		5.40		6.15
	0		12.01		11.70
10	0.5		10.90		11.27
	1		9.58		10.65
	0		8.50		8.28
20	0.5	FGX/FGO/FGX	7.71	FGX/FGA/FGX	7.97
	1		6.77		7.53
	0		6.94		6.76
30	0.5		6.29		6.51
	1		5.53		6.15

Table 8 Comparison between Mori-Tanaka's model and mixture rule

L/H	Mori-Tanaka Model	Mixture rule	Difference (%)
10	3.59E+09	3.36E+09	6.2527%
20	8.98E+08	8.41E+08	6.2511%
30	3.99E+08	3.74E+08	6.2514%

5.2 Results and discussion of vibration

The first natural frequency against porosity coefficient in three different elastic foundations is presented in Fig. 7. It should be noted that clamped boundary conditions are applied at two ends of the beam, and Kf0, and α are assumed to be 1000 and 0.2, respectively. As could be seen, constant K during the beam length has the most resistance against vibration. In the case of varying elastic foundations linearly, the natural frequency has the least amount comparing to the others. While porosity coefficients increase from 0 to 1, the first natural frequency decreases by about 20 percent. The mentioned result is almost the same for other elastic foundation variations. It is noted that with an increase in the porosity coefficient, the stiffness and mass of the sandwich beam decrease, but a decrease stiffness matrix is higher than the mass matrix, thus for this structure, the natural frequency reduces.

In Table 7, for Model 3, the natural frequency for a different combination of core and top and bottom parts of composite for three slenderness ratio and coefficient of the porosity is presented. Distributions of fibers in the matrix were considered differently using Eq. (27). FGA/FGX/FGA has the most natural frequency among other combinations. It means the structure more resistant against vibration. There is no difference if the core and top and bottom part are changed. FGX/FGO/FGX is the least resistant one against free vibration.

5.3 Comparison of Mori-Tanaka model with porosity coefficient method

In this part, instead of using the volume fraction method to model composite, the Mori-Tanaka model utilized to calculate averaged stresses and strains in the fiber and matrix materials. Mori-Tanaka's tensor by following equations.

$$[A_{ij}] = \begin{bmatrix} A_{11} & A_{12} & 0 \\ A_{21} & A_{22} & 0 \\ 0 & 0 & A_{66} \end{bmatrix} \tag{39}$$

Mori-Tanaka's elements are correlated by E and G (Young's and shear moduli of material, respectively) and v (Poisson's ratio). It should be mentioned that superscripts f and m referring to the fiber and the matrix.

$$E_{11} = \frac{\begin{matrix}(V_f + V_m A_{11})(V_f + V_m A_{22}) \\ -A_{12}A_{21}V_m^2\end{matrix}}{\begin{matrix}(V_f + V_m A_{22})(V_f S_{11}^f + V_m A_{11} S_{11}^m) \\ +V_f V_m (S_{12}^m - S_{12}^f)A_{21} - A_{12}A_{21}V_m^2 S_{11}^m\end{matrix}} \tag{40}$$

Longitudinal Young's Modulus can be obtained based on Mori-Tanaka's elements. Transversal modulus of elasticity and shear modulus also have similar relationships described. The comparison between Mori-Tanaka's model and the mixture rule is shown in Table 8. As can be seen, there is an acceptable agreement between the volume fraction method and Mori-Tanaka Model. It should be mentioned Mori-Tanaka model results make about 6% critical buckling loads higher than volume fraction theory.

Conclusions

In this research, the buckling and free vibration analysis of sandwich functionally graded composite Timoshenko beam considering porosity distribution with carbon nanotubes/ graphene platlets resting on variable elastic foundation is investigated that the obtained results have

been listed as follows

• It was concluded that porous FGM has a more critical buckling load than porous composite. Perfect FGM is also more resistant against buckling than perfect composite. By increasing the gradient index of FG material in Perfect FGM, the critical buckling load will rise substantially.

• Comparing three models about the influence of the core height on buckling load Model 3 (when the core height is eight times of top part height) has the most critical buckling load.

• It was also shown with considering porosity coefficient that the critical buckling load and natural frequency decreases linearly by increasing the porosity coefficient in distribution Type 1. It should be noted the amount of decrease has an inverse relationship with the aspect ratio of beam.

• It was also concluded that in the case of assuming porosity distribution Type 2, the beam has the most resistance against buckling and vibration. In contrast, the beam with the distribution of porosity Type 1 has the minimum critical buckling load and the natural frequency among three other porosity patterns.

• Among the three discussed elastic foundations, the buckling load, and natural frequency in linear variation during length have the least amount comparing to the others.

• When the porosity coefficients increase from 0 to 1, the critical buckling load and first natural frequency decrease by about 55 and 20 percent, respectively.

• It was shown that FGX/FGO/FGX combination has the most natural frequency among the others. In contrast, FGO/FGX/FGO is the least resistant one against free vibration.

• Mori-Tanaka model results make about 6% critical buckling loads higher than volume fraction theory.

Acknowledgment

The authors would like to thank the referees for their valuable comments. Also, they would like to thank the Iranian Nanotechnology Development Committee for their financial support and the University of Kashan for supporting this work by Grant No. 891238/19.

References

Akbaş, Ş.D. (2017), "Vibration and static analysis of functionally graded porous plates", *J. Appl. Computat. Mech.*, **3**(3), 199-207. https://doi.org /10.22055/JACM.2017.21540.1107.

Akbaş, Ş.D. (2018), "Forced vibration analysis of functionally graded porous deep beams", *Compos. Struct.*, **186**, 293-302. https://doi.org/10.1016/j.compstruct.2017.12.013.

Akbaş, S.D. (2020), "Modal analysis of viscoelastic nanorods under an axially harmonic load", *Adv. Nano Res., Int. J.*, **8**(4), 277-282. https://doi.org/10.12989/anr.2020.8.4.277.

Analooei, H.R., Azhari, M., Heidarpour, A., Ng, T.Y. and Lin, R.M. (2013), "Elastic buckling and vibration analyses of orthotropic Nano plates using nonlocal continuum mechanics and spline finite strip method", *Appl. Math. Model.*, **37**(10-11), 6703-6717. https://doi.org/10.1016/j.commatsci.2012.06.031.

Anirudh, B., Ganapathi, M., Anant, C. and Polit, O. (2019), "A comprehensive analysis of porous graphene-reinforced curved beams by finite element approach using higher-order structural theory: Bending, vibration and buckling", *Compos. Struct.*, **222**, 110899. https://doi.org /10.1016/j.compstruct.2019.110899.

Ansari, R. and Sahmani, S. (2011), "Surface stress effects on the free vibration behavior of nanoplates", *Int. J. Eng. Sci.*, **49**(11), 1204-1215. https://doi.org/10.1016/j.ijengsci.2011.06.005.

Arefi, M., Kiani, M. and Rabczuk, T., (2019) "Application of nonlocal strain gradient theory to size dependent bending analysis of a sandwich porous nanoplate integrated with piezomagnetic face-sheets", *Compos. Part B-Eng.*, **168**, 320-333. https://doi.org/10.1016/j.compositesb.2019.02.057.

Bessaim, A., Ahmed Houari, M.S., Abdelmoumen Anis, B., Kaci, A., Tounsi, A. and Adda Bedia, E.A. (2018), "Buckling analysis of embedded nanosize FG beams based on a refined hyperbolic shear deformation theory", *J. Appl. Computat. Mech.*, **4**(3), 140-146. https://doi.org/10.22055/JACM.2017.22996.1146.

Chen, D., Yang, J. and Kitipornchai, S. (2015), "Elastic Buckling and Static Bending of Shear Deformable Functionally Graded Porous Beam", *Compos. Struct.*, **133**, 54-61. https://doi.org/10.1016/j.compstruct.2015.07.052.

Chen, D., Kitipornchai, S. and Yang, J. (2017) "Free vibration and elastic buckling of functionally graded porous beams reinforced by graphene platelets", *Mater. Des.*, **116**, 656-665. https://doi.org/10.1016/j.matdes.2016.12.061.

Chen, X.C., Chen, L., Huang, S., Li, M. and Li, X. (2021), "Nonlinear forced vibration of in-plane bi-directional functionally graded materials rectangular plate with global and localized geometrical imperfections", *Appl. Math. Model.*, **93**, 443-466. https://doi.org/10.1016/j.apm.2020.12.033.

Chikr, C., Kaci, A., Yeghnem, R. and Tounsi, A. (2019), "A new higher-order shear and normal deformation theory for the buckling analysis of new type of FGM sandwich plates", *Struct. Eng. Mech., Int. J.*, **72**(5), 653-673. https://doi.org/10.12989/sem.2019.72.5.653.

Demirhan, P.A. and Taskin, V. (2019), "Bending and free vibration analysis of Levy-type porous functionally graded plate using state space approach", *Compos. Part B-Eng.*, **160**, 661-676. https://doi.org/10.1016/j.compositesb.2018.12.020.

Ebrahimi, F., Nouraei, M., Dabbagh, A. and Civalek, O. (2019), "Buckling analysis of graphene oxide powder-reinforced nanocomposite beams subjected to non-uniform magnetic field", *Struct. Eng. Mech., Int. J.*, **71**(4), 351-361. https://doi.org/10.12989/sem.2019.71.4.351.

Gao, Y., Xiao, W.S. and Zhu, H. (2019), "Nonlinear vibration of functionally graded nano-tubes using nonlocal strain gradient theory and a two-steps perturbation method", *Struct. Eng. Mech., Int. J.*, **69**(2), 205-219. https://doi.org/10.12989/sem.2019.69.2.205.

Halpin, J.C. and Tsai, S.W. (1967), "Environmental Factors in Composite Materials Design", *U.S. Air Force Technical Report AFML TR*, 67423.

Hosseini-Hashemi, S., Bedroud, M. and Nazemnezhad, R. (2013), "An exact analytical solution for free vibration of functionally graded circular/annular Mindlin nanoplates via nonlocal elasticity", *Compos. Struct.*, **103**, 108-118. https://doi.org /10.1016/j.compstruct.2013.02.022.

Jabbari, M., Mojahedin, A., Khorshidvand. A.R. and Eslami, M.R. (2013). "Buckling analysis of a functionally graded thin circular plate made of saturated porous materials", *J. Eng. Mech.*, **140**(2), 287-295. https://doi.org/10.1061/(asce)em.1943-7889.0000663.

Jabbari, M., Hashemitaheri, M., Mojahedin, A. and Eslami, M.R. (2014), "Thermal buckling analysis of functionally graded thin circular plate made of saturated porous materials", *J. Therm. Stresses*, **37**(2), 202-220. https://doi.org/10.1080/01495739.2013.839768.

Jabbari, M. and Rezaei, M. (2016), "Mechanical Buckling of FG

Saturated Porous Rectangular Plate with Piezoelectric Actuators", *Iran. J. Mech. Eng*., **17** (2), 45-65.

Karami, B. and Karami, S. (2019), "Buckling analysis of nanoplate-type temperature-dependent heterogeneous materials", *Adv. Nano Res., Int. J.*, **7**(1), 51-61. https://doi.org/10.12989/anr.2019.7.1.051.

Kim, J., Kamil Żur, K. and Reddy, J.N. (2019), "Bending, free vibration, and buckling of modified couples stress-based functionally graded porous micro-plates", *Compos. Struct*., **209**, 879-888. https://doi.org/10.1016/j.compstruct.2018.11.023.

Li, L., Li, X. and Hu, Y. (2016), "Free vibration analysis of nonlocal strain gradient beams made of functionally graded material", *Int. J. Eng. Sci*., **102**, 77-92. https://doi.org/10.1016/j.ijengsci.2016.02.010.

Li, L., Tang, H. and Hu, Y. (2018), "The effect of thickness on the mechanics of nanobeams", *Int. J. Eng. Sci.*, **123**, 81-91. https://doi.org/10.1016/j.ijengsci.2017.11.021.

Li, X. (2021), "Parametric resonances of rotating composite laminated nonlinear cylindrical shells under periodic axial loads and hydrothermal environment", *Compos. Struct*., **255**, 112887. https://doi.org/10.1016/j.compstruct.2020.112887.

Liu, L. and Huang, Z. (2014), "A note on Mori-Tanaka's method", *Acta Mech. Solida Sin*., **27**(3), 234-244. https://doi.org/10.1016/S0894-9166(14)60033-1.

Magnucka-Blandzi, E. (2008), "Axisymmetrical deflection and buckling of circular porous-cellular plate", *Thin Wall. Struct*., **46**, 333-337. https://doi.org /10.1016/j.tws.2007.06.006.

Magnucki, K., Malinowski, M. and Kasprzak, J. (2006) "Bending and Buckling of a Rectangular Porous Plate", *Steel Compos. Struct*., *Int. J.*, **6**(4), 319-333. https://doi.org/10.12989/scs.2014.16.3.325.

Malekzadeh, P., Setoodeh, A.R. and Beni, A.A. (2011), "Small scale effect on the thermal buckling of orthotropic arbitrary straight-sided quadrilateral nanoplates embedded in an elastic medium", *Compos. Struct*., **93**, 2083-2089. https://doi.org/10.1016/j.compstruct.2011.02.013.

Mehrabi, M., Mohammadimehr, M. and Mousavinejad, F.S. (2021), "2D magneto-mechanical vibration analysis of a micro composite Timoshenko beam resting on orthotropic medium", *Smart Struct. Syst*., *Int. J.*, **27**(1), 1-18. http://dx.doi.org/10.12989/sss.2021.27.1.001.

Mohamed, N., Eltaher, M.A., Mohamed, S.A. and Seddek, L.F. (2019), "Energy equivalent model in analysis of postbuckling of imperfect carbon nanotubes resting on nonlinear elastic foundation", *Struct. Eng. Mech., Int. J.*, **70**(6), 737-750. https://doi.org/10.12989/sem.2019.70.6.737.

Mohammadimehr, M., Afshari, H., Salemi, M., Torabi, K. and Mehrabi, M. (2019), "Free vibration and buckling analyses of functionally graded annular thin sector plate in-plane loads using GDQM", *Struct. Eng. Mech., Int. J.*, **71**(5), 525-544. https://doi.org/10.12989/sem.2019.71.5.525.

Mohammadimehr, M., Mehrabi, M. and Mousavinejad, F.S. (2020), "Magneto-mechanical vibration analysis of single-/three-layered micro-Timoshenko porous beam and graphene platelet as reinforcement based on modified strain gradient theory and differential quadrature method", *J. Vib. Contr*., 1077546320949083. https://doi.org/10.1177/1077546320949083.

Murmu, T., McCarthy, M.A. and Adhikari, S. (2013), "In-plane Magnetic Field Affected Transverse Vibration of Embedded Singlelayer Graphene Sheets using Equivalent Nonlocal Elasticity Approach", *Compos. Struct*., **96**, 57-63. https://doi.org/10.1016/j.compstruct.2012.09.005.

Natarajan, S., Chakraborty, S., Thangavel, M., Bordas, S. and Rabczuk, T. (2012), "Size-dependent free flexural vibration behavior of functionally graded nanoplates", *Computat. Mater. Sci*., **65**, 74-80. https://doi.org/10.1016/j.commatsci.2012.06.031.

Nejadi, M.M. and Mohammadimehr, M. (2020), "Buckling analysis of nano composite sandwich Euler-Bernoulli beam considering porosity distribution on elastic foundation using DQM", *Adv. Nano Res., Int. J.*, **8**(1), 59-68. https://doi.org/10.12989/anr.2020.8.1.059.

Nejadi, M.M., Mohammadimehr, M. and Mehrabi, M. (2021), "Free vibration and stability analysis of sandwich pipe by considering porosity and graphene platelet effects on conveying fluid flow", *Alexandria Eng. J.*, **60**(1), 1945-1954. https://doi.org/10.1016/j.aej.2020.11.042.

Noroozi, R., Barati, A., Kazemi, A., Norouzi, S. and Hadi, A. (2020), "Torsional vibration analysis of bi-directional FG nano-cone with arbitrary cross-section based on nonlocal strain gradient elasticity", *Adv. Nano Res., Int. J.*, **8**(1), 13-24. https://doi.org/10.12989/anr.2020.8.1.013.

Polit, O., Anant, C., Anirudh, B. and Ganapathi, M. (2019), "Functionally graded Graphene reinforced porous nanocomposite curved beams: Bending and elastic stability using a higher-order model with thickness stretch effect", *Compos. Part B-Eng*., **166**, 310-327. https://doi.org/10.1016/j.compositesb.2018.11.074.

Radić, N. (2018), "On buckling of porous double-layered FG nanoplates in the Pasternak elastic foundation based on nonlocal strain gradient elasticity", *Compos. Part B-Eng*., **153**, 456-479. https://doi.org /10.1016/j.compositesb.2018.09.014.

Shahsavari, D., Karami, B. and Mansouri, S. (2018), "Shear buckling of single layer graphene sheets in hygrothermal environment resting on elastic foundation based on different nonlocal strain gradient theories", *Eur. J. Mech. A-Solid*., **67**, 200-214. https://doi.org /10.1016/j.euromechsol.2017.09.004.

Shariati, A., Barati, M.R., Ebrahimi, F., Singhal, A. and Toghroli, A. (2020), "Investigating vibrational behavior of graphene sheets under linearly varying in-plane bending load based on the nonlocal strain gradient theory", *Adv. Nano Res., Int. J.*, **8**(4), 265-276. https://doi.org/10.12989/anr.2020.8.4.265.

She, G.L., Ren, Y.R., Yuan, F.G. and Xiao, W.S. (2018), "On vibrations of porous nanotubes", *Int. J. Eng. Sci*., **125**, 23-35. https://doi.org /10.1016/j.ijengsci.2017.12.009.

She, G.L., Yuan, F.G. and Ren, Y.R. (2018), "On wave propagation of porous nanotubes", *Int. J. Eng. Sci*., **130**, 62-74. https://doi.org/10.1016/j.ijengsci.2018.05.002.

She, G.L., Yuan, F.G., Karami, B., Ren, Y.R. and Xiao, W.S. (2019), "On nonlinear bending behavior of FG porous curved nanotubes", *Int. J. Eng. Sci*., **135**, 58-74. https://doi.org/10.1016/j.ijengsci.2018.11.005.

Sobhy, M. and Zenkour, A.M. (2019), "Porosity and inhomogeneity effects on the buckling and vibration of double-FGM nanoplates via a quasi-3D refined theory", *Compos. Struct*., **220**, 289-303. https://doi.org/10.1016/j.compstruct.2019.03.096.

Taborda, C.S., Bernardo, L. and Gama, J. (2018), "Effective torsional strength of axially restricted RC beams", *Struct. Eng. Mech., Int. J.*, **67**(5), 465-479. https://doi.org/10.12989/sem.2018.67.5.465.

Tang, H., Li, L. and Hu, Y. (2018), "Buckling analysis of two-directionally porous beam", *Aerosp. Sci. Technol*., **78**, 471-479. https://doi.org/10.1016/j.ast.2018.04.045.

Tang, H., Li, L. and Hu, Y. (2019), "Coupling effect of thickness and shear deformation on size-dependent bending of micro/nano-scale porous beams", *Appl. Math. Model*., **66**, 527-547. https://doi.org/10.1016/j.apm.2018.09.027.

Timoshenko, S. and Young, D.H. (1995), *Vibration Problems in Engineering*, VanNostrand Company, New York, U.S.A.

CC